American Transactions on
Engineering & Applied Sciences

http://TuEngr.com/ATEAS

Computer Modeling and Optimization of Swage Autofrettage Process of a Thick-Walled Cylinder Incorporating Bauschinger Effect

Zhong Hu [a*] and Chandra Penumarthy [a]

[a] *Department of Mechanical Engineering, South Dakota State University, USA*

ARTICLEINFO

Article history:
Received December 02, 2013
Received in revised form
January 06, 2014
Accepted January 10, 2014
Available online
January 14, 2014

Keywords:
Nonlinear
Strain-hardening;
Finite Element
Analysis;
Residual Stress.

ABSTRACT

In this paper, the swage autofrettage process of a thick-walled cylinder has been numerically investigated. The corresponding axi-symmetric finite element model has been developed. The elasto-plastic material model with nonlinear strain-hardening and kinematic hardening (the Bauschinger effect) was adopted. The residual stresses in the thick-walled cylinder induced by swage autofrettage process have been analyzed. The residual stresses by modeling have been compared with the experimental results from the literature. The influences of the Bauschinger effect and friction on stress and strain distribution have been evaluated. The optimum mandrel dimensions (percent radial interference) and the maximum percent reduction of the von Mises stress in the swaged autofrettaged thick-walled cylinder under the elastic-limit working pressure have been found.

1. Introduction

Thick-walled cylinders subjected to constant or cyclic high internal pressure and/or elevated temperature are widely used in the nuclear and chemical industries involving pressures as high as 1380 MPa and temperatures of up to 300°C [1], especially for military applications involving

*Corresponding author (Z. Hu). Tel/Fax: +1-605-688-4817/+1-605-688-5878. E-mail address: Zhong.Hu@sdstate.edu. ©2014. American Transactions on Engineering & Applied Sciences. Volume 3 No. 1 ISSN 2229-1652 eISSN 2229-1660 Online Available at http://TuEngr.com/ATEAS/V03/0031.pdf .

transient peak internal pressures as high as 350 MPa and temperature of up to 1500°C inside the gun barrel in a ballistic event [2]. In the absence of residual stresses, cracks usually form at the bore where the hoop stress developed by the working pressure is highest [3-6]. In order to prevent such failure so as to prolong fatigue life or to increase the pressure-carrying capacity, favorable compressive residual hoop stresses are introduced to the inner portion of the cylinder, commonly by the autofrettage processes prior to use. Autofrettage is a material fabrication process in which a cylinder vessel is subjected to sufficient internal pressure so that part or all of the wall thickness is stressed beyond the elastic limit and produce permanent (plastic) deformation. When unloaded, the inner layer of the wall is circumferentially compressed while the outer layer remains in circumferential (hoop) tension. When the cylinder is internally pressurized in service, these residual compressive hoop stresses at the bore are partially canceling the tensile hoop stresses generated by the working pressures and thus lower the equivalent stress and prolong the fatigue life. The permanent deformation of the bore of a cylinder induced by the autofrettage processes can be produced by the direct application of hydraulic pressure to the bore. High pressures close to failure in the range of 1000 to 2000MPa were necessary. However, the hydraulic autofrettage process was slow, expensive, and dangerous. An alternative technique is swage autofrettage. The process is carried out by pushing a plain or a profiled oversized mandrel (or swage) through inside a thick-walled cylinder, thereby causing gradually plastic deformation from one end to the other end to the inner surface layer by mechanical interference [7-10]. Thus, it requires much smaller axial force for driving the ram (swage) than that required in conventional hydraulic autofrettage [7], and is energy efficient. However, the equipment requirements are still significant and the axial force required for driving the ram increases with the size of the cylinder, and furthermore, the interaction between the mandrel and the bore surface are more complicated. It is therefore an advantage to minimize the axial force requirement and produce the best favorable compressive hoop stresses.

In general, vessels under high pressure require a strict analysis for secure operational performance. Prediction of residual stress field and optimization of the autofrettage process parameters are some of the key issues which normally involve a careful evaluation by experiments, analytical analysis, or computational modeling. Davidson et al. [8] were the first to measure, in a series of experiments, the residual stress field due to swage autofrettage using the destructive Sachs boring method. In Lee's report [11,12], the position-sensitive x-ray diffraction techniques were applied to characterize residual stresses (hoop and radial stresses) in pre-pressurized thick-walled swaged autofrettaged cylinders. In order to validate the numerical

results, Perl and Perry have used strain gages to measure the actual strains and the mandrel's pushing force during a standard swage autofrettage process [13]. Experimental investigation is a reliable approach if the details of the mandrel's insertion into the cylinder could be measured correctly so that the effects of the mandrel parameters on the production of the residual stresses could be analyzed and then the process could be optimized. However, experimental approach is very expensive and time consuming, and it is impossible to repeat a lot of tests for measuring the residual stress and for finding the optimal process parameters, instead, it may be used as a validation tool for analytical or numerical solutions [10-16]. Moreover, the real-time measurements can only be done on the surface of the cylinder. In case of 3-D measurement, slices of the tube need to be cut from the cylinder, machine polish, and then electropolish. Surface material removal is made so that the effects due to sanding, machining, and oxidation will not influence the residual stress measurements. However, since the residual stresses induced by swage autofrettage is three dimensional, and large compressive axial and hoop stresses near the inner surface of the cylinder will be presented due to the compressive deformation nature. Cutting slices from the cylinder will completely release the axial compressive stress resided on the surfaces of the slices, and therefore cause redistribution of the residual hoop stress as well as the residual radial stress. This testing sample preparation process will cause noticeable error. Analytical or theoretical solution of the swage autofrettage of a constant cross-section cylinder is possible only through the use of simplifying assumptions, such as choice of yield criteria and material compressibility and, critically, material stress-strain behavior [10,13,14,17,18]. On the other hand, swage autofrettage proceeds from one end to the other end and gradually causes large localized plastic strains around the inner surface of a cylinder, which noticeably causes the early onset of non-linearity when remove the swage pressure in the unloading process - a kinematic hardening phenomenon termed the Bauschinger effect (BE). This non-linearity typically causes significant deviation from those material models that are often assumed. The effect is most pronounced around the inner surface, and in turn has a significant effect on the residual stresses developed after the swage autofrettage load is removed, especially as it can cause reverse yielding to occur when it otherwise would not be expected. Research has been done on this issue with theoretical analysis mostly based on bilinear kinematic hardening (linear elastic and linear hardening) material model which is a good approximation for small strain, and theoretical solution only capable for internal pressurized autofrettage process which is uniform and symmetric deformation for an axi-symmetric model [10,13,19-26]. However, the practical material model is of nonlinear

*Corresponding author (**Z. Hu**). Tel/Fax: +1-605-688-4817/+1-605-688-5878. E-mail address: Zhong.Hu@sdstate.edu. Volume 3 No. 1 ISSN 2229-1652 eISSN 2229-1660 Online Available at http://TuEngr.com/ATEAS/V03/0031.pdf .

kinematic hardening and with equivalent strain up to 5% in the swage autofrettage process. Furthermore, deformation during swage autofrettage is localized, axi-symmetric and dynamic process moving from one end to the other end. All these give complexity to theoretical analysis on a complex material processes like swage autofrettage.

Computer modeling techniques based on finite element analysis (FEA) provides a powerful alternative for analyzing and optimizing the swage autofrettage processes [13,14,16,17,19,20,27-30]. The typical work on the incorporation of variable BE into FEA modeling started as earlier as in 1980s, such as Chaaban [19] and Chaaban et al. [20], in which they used a FEA to model the residual stress in an autofrettaged thick-walled high pressure vessel, considering the Bauschinger effect factor (BEF). Perl and Perry [13] derived an analytical solution based on small strain and incorporated BE on the yield stress and Young's modulus, and the mathematical model was finally solved by the finite difference method. For a sample cylinder with an inner radius of 60mm and an outer radius of 100mm under a friction coefficient of 0.33 and a radial interference of 1.62mm (2.7% interference), the discrepancy between the experimental value of the pushing force (4710 kN) and the predicted force (4900 kN) is 4%. While for a smaller radial interference of 0.57mm (0.95% interference), the discrepancy is 6%, i.e., calculated force of 1600kN versus measured force of 1700kN. Iremonger [27] and Parker et al. [15] incorporated in their analysis only the basic yield strength effect through BEF, experimentally determined by Milligan et al. [31]. Iremonger [27], using FEA, was able to determine the mandrel's pushing force to within 25%. O'Hara [32] conducted a full swage autofrettage problem modeling, excluded BE from his model. In Perry and Perl's work [14], the axi-symmetric equilibrium equations, in terms of radial and axial displacements, were approximated by finite differences and solved by Gauss-Seidel method. The calculated strains, the permanent bore enlargement, and the mandrel pushing force were found to be in agreement with the measured values. Even though, numerical models of autofrettage were validated in certain level by different experimental methods, such as neutron diffraction [33], Sachs boring [8,33], the compliance method [33] deep-hole technique [34], the position-sensitive x-ray diffraction techniques[11,12], the strain gages [13], to mention a few. All these experimental methods, in certain degree having fatal defect, were aimed at measuring the prevailing residual stress field or part of it, but none of them is capable of providing the complete process design and optimization via process parameter investigation. As input for the numerical analysis of the residual stresses due to swage autofrettage, nonlinear stress-strain data with BE as well as other appropriate material properties can be easily implemented. However, since BE is found to be a function of the prior plastic strain, especially for high strength pressure

vessel materials [17,35-43], it is still lack of adequate analysis and optimization of the swage autofrettage process.

In this paper, the swage autofrettage process of a thick-walled cylinder will be numerically investigated. The corresponding axi-symmetric finite element model will be developed. The elasto-plastic material model with nonlinear strain-hardening will be adopted, incorporating BE. The effects of percent radial interference on the induced residual stresses throughout the wall-thickness of the cylinder will be evaluated. The modeling residual stresses will be compared with the experimental data from literatures. The effects of BE and friction will also be analyzed. The percentage of stress reduction by swage autofrettage treatment will be calculated based on von Mises yield criterion. The optimum mandrel size and the maximum reduction percentage of the stress in the swaged autofrettaged thick-walled cylinder under the elastic-limit working pressure will be found.

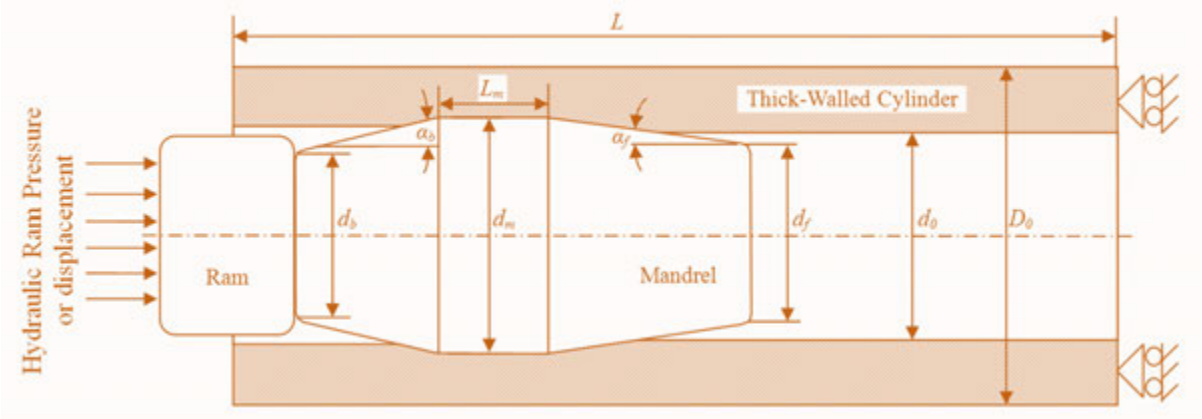

Figure 1: Geometric representation of a swage autofrettage process.

Table 1: The dimensions of the cylinder and the mandrel.

D_0 (mm)	d_0 (mm)	L(mm)	d_f(mm)	d_m (mm)	d_b (mm)	L_m (mm)	α_f(°)	α_b(°)
304.8(12)	113.8(4.48)	406.4(16)	0.99d_m	1.025 d_0	0.99d_m	0.06d_m	1.5	3

Note: Data inside parenthesis are in unit of inch (dimensions for 2.5% interference).

2. Swage Autofrettage Process Design

A thick-walled cylinder (manufactured for a 105mm cannon barrel) was used with initial internal diameter d_0 and external diameter D_0. The basic geometry of the mandrel is shown schematically in Figure1. The front (entry) diameter of the mandrel is d_f. The diameter increases, at a slop of α_f angle to the horizontal, to a maximum diameter of d_m. This maximum diameter is

*Corresponding author (Z. Hu). Tel/Fax: +1-605-688-4817/+1-605-688-5878. E-mail address: Zhong.Hu@sdstate.edu. Volume 3 No. 1 ISSN 2229-1652 eISSN 2229-1660 Online Available at http://TuEngr.com/ATEAS/V03/0031.pdf .

maintained constant over a L_m section length, beyond which it reduces at a slop of α_b angle to the horizontal until a rear diameter d_b. After the swage autofrettage treatment, the internal diameter of the cylinder expands to d. The cylinder and the mandrel diameters at entry ensure that the mandrel is well seated in the barrel prior to being driven in further. The maximum radial "interference" between the cylinder and the mandrel can be varied and optimized, depending on the residual stresses developed. The dimensions of the cylinder and the mandrel for 2.5% radial interference are listed in Table 1.

In this work, the thick-walled cylinder is made of high pressure vessel steel of ASTM A723-1130, which is usually rotary forged, heat hardened through austenizing and quenching process, tempered to improve toughness, rough and fine machined, and then swage autofrettaged, beam straightened, and thermally soaked to obtain desirable residual stress distributions. Assuming the cylinder material is of homogeneous and isotropic nonlinear hardening, and BE is an implicit function of prior plasticity. The true-stress and true-strain data [35-38] during the loading and unloading/reversed loading process can be well represented by different elasto-power law plastic models, in which the true stress - true strain behavior of the strain hardening material follows the Hooke's law in the elastic region. The true-stress and true-strain elasto-plastic with BE can be represented by the following equations:

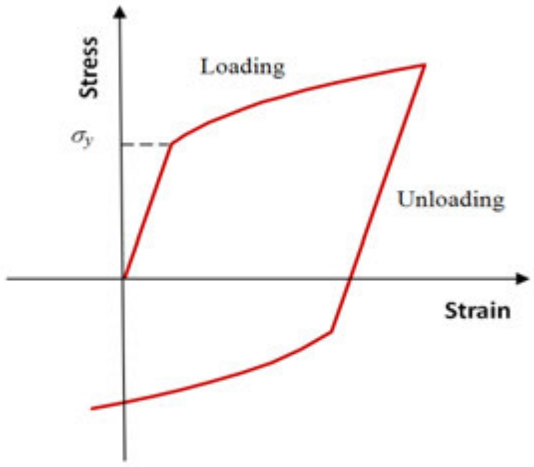

Figure 2: The elasto-plastic stress - strain model with kinematic hardening (the Bauschinger effect).

For loading:

$$\sigma = \begin{cases} E\epsilon & \epsilon < \epsilon_y \\ \sigma_y + K(\epsilon - \epsilon_y)^n & \epsilon \geq \epsilon_y \end{cases} \quad (1)$$

Where σ and ϵ are true stress and true strain, respectively. ϵ_y is the strain at the yield point. E is the modulus of elasticity. K and n are material constant and strain-hardening exponent ($0 \le n < 1$), respectively, while yield stress is

$$\sigma_y = E\epsilon_y. \quad (2)$$

For unloading/reversed loading see Figure 2.

Table 2 lists the basic material data and derived material parameters to be used in the FEA modeling [17, 32, 37-43].

Table 2: Material properties of the Cylinder, Mandrel and Ram [17,32, 37-43].

Component	Cylinder	Mandrel	Ram
Material	ASMT A723-1130 [17]	Tungsten Carbide	HS carbon steel
Modulus of Elasticity E	209 GPa	500 GPa	209GPa
Poisson's Ratio υ	0.30	0.24	0.3
Yield Strength σ_y	1068 MPa		
0.1% Yield Strength σ_y	1130 MPa		
Strain at Yield Point ϵ_y	5.1×10^{-3}		
Ultimate Tensile strength	1256 MPa		

For validating the material model used in the following modeling and verifying the effect of the BE, several modeling tests have been done, including an uni-axial tensile and compression test, and bore hoop stress investigation in an open-end pressurized autofrettage thick-walled cylinder [44,45].

Table 3: Friction coefficients used in the model.

Contact interface	Friction coefficient
Ram-mandrel contact	0.05
Cylinder-mandrel contact	0.015

The force required for pushing the mandrel forward is determined by elasto-plastic deformation and the friction generated by the mandrel interacting with the bore surface. The friction coefficients between the ram and the mandrel and between mandrel and cylinder are listed in Table 3 [17,32], in which the exact value of friction between the ram and the mandrel has little effect because of the low relative sliding on this interface. However, the interface between the mandrel and the bore surface is critical because it is the location of the moving contact surface, and is the major contributor to the driving force of the swage autofrettage process. A coefficient of friction of 0.015 was used to model this interface which was lubricated by a sterate-based high

*Corresponding author (Z. Hu). Tel/Fax: +1-605-688-4817/+1-605-688-5878. E-mail address: Zhong.Hu@sdstate.edu.

Volume 3 No. 1 ISSN 2229-1652 eISSN 2229-1660 Online Available at http://TuEngr.com/ATEAS/V03/0031.pdf .

pressure lubricant held in place by a porous phosphate coating [32].

3. Model Set-Up

In general, the swage autofrettage process can be properly treated as an axi-symmetric problem. The commercially available software ANSYS has been used for finite element modeling of the swage autofrettaged thick-walled cylinder [46]. The finite element model is shown in Figure 3. The element type of PLANE183 has been adopted, which is an eight-node 2-D axi-symmetric element with the capacity of elastic and plastic material nonlinearity and non-linear BEF. Since the deformation during the swage autofrettage process is primary concentrated near the bore, for modeling accuracy, more elements were used near the bore and the contacting segment of the mandrel, see Figure 3. For modeling the contact between the mandrel outer surface vs. the cylinder inner surface, as well as the mandrel top surface vs. the ram bottom surface, a surface-to-surface contact model was used, in which 2-D axi-symmetric target segment TARGE169 and contact element CONTA172 were employed. TARGE169 was used to represent various "target" surfaces for the associated contact elements. Contact occurs when the element surface penetrated one of the target segment elements on a specified target surface. Coulomb friction was considered in the modeling. The proper element size and total element number were determined through convergence study of the von Mises stress, an indicator considering the contribution of every stress component, all over the cylinder, especially the maximum von Mises stress in the mid-length cross-section of the cylinder which will be used later to determine the reduction of the final stress in the cylinder under the maximum working pressure. The convergence study shows that the stresses are mesh independent when total elements reach the number indicated in Table 4, in which the approximate error is much less than 1%.

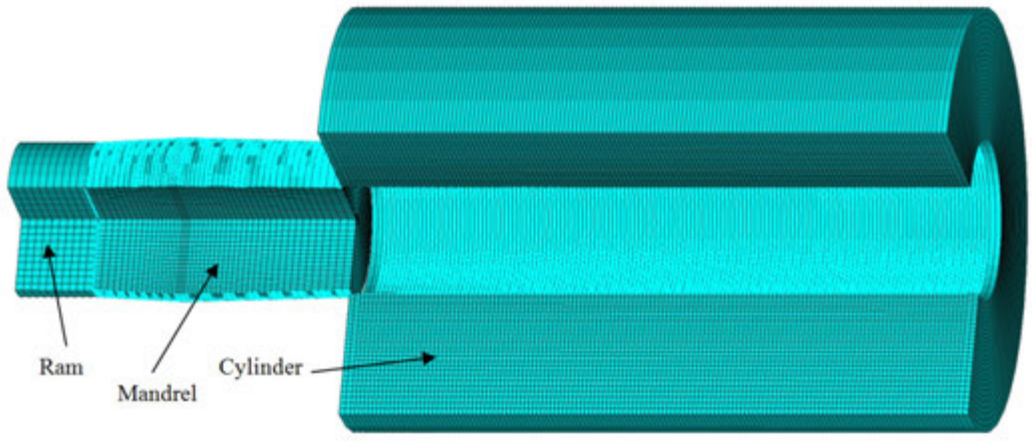

Figure 3: Finite element model for swage autofrettage of an axi-symmetric thick-walled cylinder (2-D model expanded axi-symmtrically for display).

Table 4: Total number of elements and nodes used in the modeling.

Element type	Number of elements/nodes
Solid element:	
Cylinder element PLANE183	4,032
Mandrel element PLANE183	936
Ram element PLANE183	100
Contact Element: TARGE169/CONTA172	220
Total Number of elements	5,288
Total Number of Nodes	15,731

4. Modeling Results and Discussion

4.1 Pressurizing cylinder by maximum working pressure without swage autofrettage

Consider a thick-walled cylinder having inner radius *a* and outer radius *b* and subjected to the internal pressure p_i. The material will obey the Hooke's law when it is within the elastic region. This allow us to use the Lame's equations for calculating the hoop stress, σ_θ, and radial stress, σ_r, along the wall-thickness of the cylinder, when the ends of the cylinder are open and unconstrained so that the cylinder is in a condition of plane stress [26,47].

$$\sigma_\theta = \frac{a^2 p_i}{b^2 - a^2}\left[1 + \left(\frac{b^2}{r^2}\right)\right] \tag{3}$$

$$\sigma_r = \frac{a^2 p_i}{b^2 - a^2}\left[1 - \left(\frac{b^2}{r^2}\right)\right] \tag{4}$$

$$\sigma_z = 0 \tag{5}$$

Therefore, the von Mises (equivalent) stress is

$$\sigma_i = \left(\sigma_\theta^2 + \sigma_r^2 - \sigma_\theta \sigma_r\right)^{\frac{1}{2}} = \frac{a^2 p_i}{b^2 - a^2}\left[1 + 3\left(\frac{b}{r}\right)^4\right]^{\frac{1}{2}} \tag{6}$$

The radial displacement is

$$u = \frac{a^2 p_i r}{E(b^2 - a^2)}\left[(1 - \nu) + (1 + \nu)\frac{b^2}{r^2}\right] \tag{7}$$

Obviously, the maximum von Mises stress is at inner surface, $r = a$. Assuming von Mises yield criterion applied, i.e., $\sigma_i \leq \sigma_y$, so by substituting the data from Table 1 and Table2, the

*Corresponding author (Z. Hu). Tel/Fax: +1-605-688-4817/+1-605-688-5878. E-mail address: Zhong.Hu@sdstate.edu.

Volume 3 No. 1 ISSN 2229-1652 eISSN 2229-1660 Online Available at http://TuEngr.com/ATEAS/V03/0031.pdf .

maximum applied working pressure (the maximum internal pressure without causing yielding) is

$$p_{max} = \sigma_y \frac{b^2-a^2}{a^2}\left[1+3\left(\frac{b}{a}\right)^4\right]^{-\frac{1}{2}} = 529.0 \text{ (MPa)} \quad (8)$$

Figure 4 shows the analytical and modeling results of stress components and radial displacement along the thickness of the cylinder subjected to the maximum working pressure (p_{max} = 529.0 MPa). The modeling results are well agreed with the analytical results from Lame's equations, indicating the reliability of the model employed in the numerical analysis. Figure4 also shows that the maximum von Mises stress and hoop stress located at the inner surface of the cylinder, and the hoop stress is the major stress component causing yield failure.

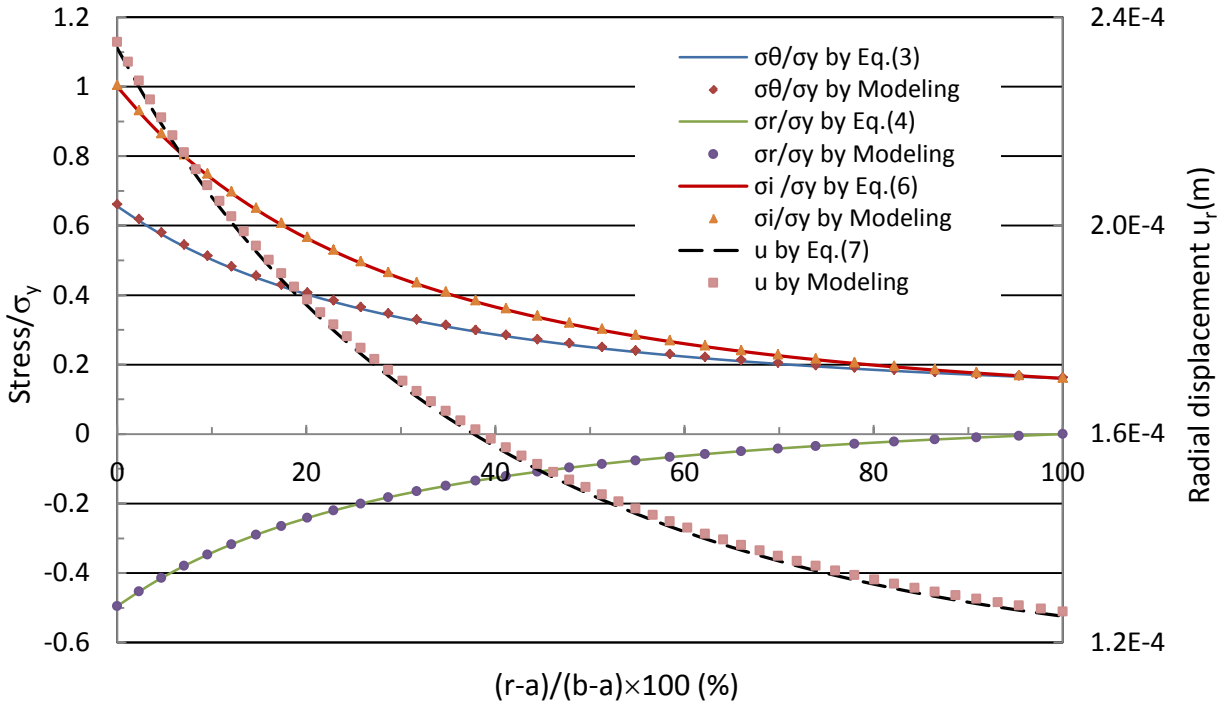

Figure 4: Analytical and modeling results of stresses and radial displacement along the wall-thickness of the cylinder subjected to the maximum working pressure (p_{max} = 529.0 MPa).

4.2 Residual stresses by swage autofrettage

Swage autofrettage process is a localized and dynamic deformation process. Figs. 5 and 6 show the contour plots of the stress (radial, hoop, axial, and von Mises) components and the von Mises plastic strain developing when the mandrel moved to the mid-way of the process considering BE from Figure 2 and friction coefficients from Table 3 for the case of 2.5% radial interference. Figs. 7 and 8 show the contour plots of the residual stress (radial, hoop, axial and von Mises) components and residual von Mises plastic strain developed after completing swage autofrettage

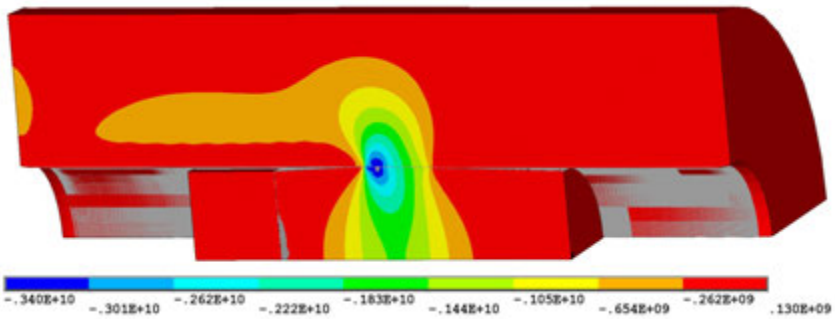

(a) Radial stress

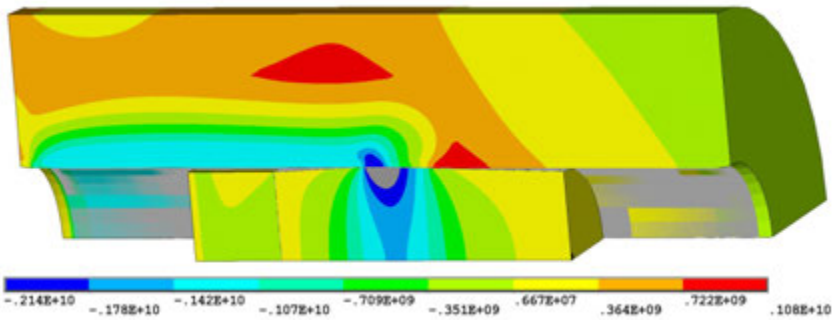

(b) Hoop stress

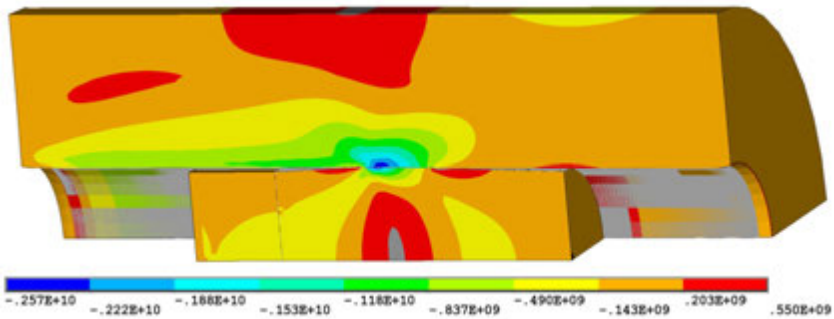

(c) Axial stress

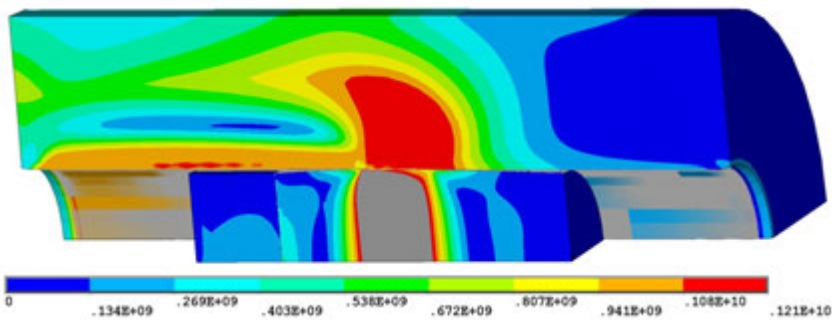

(d) von Mises stress

Figure 5: Stress (Pa) distribution at the mid way of the swage autofrettage (2.5% interference with BE & friction).

*Corresponding author (**Z. Hu**). Tel/Fax: +1-605-688-4817/+1-605-688-5878. E-mail address: Zhong.Hu@sdstate.edu. Volume 3 No. 1 ISSN 2229-1652 eISSN 2229-1660 Online Available at http://TuEngr.com/ATEAS/V03/0031.pdf .

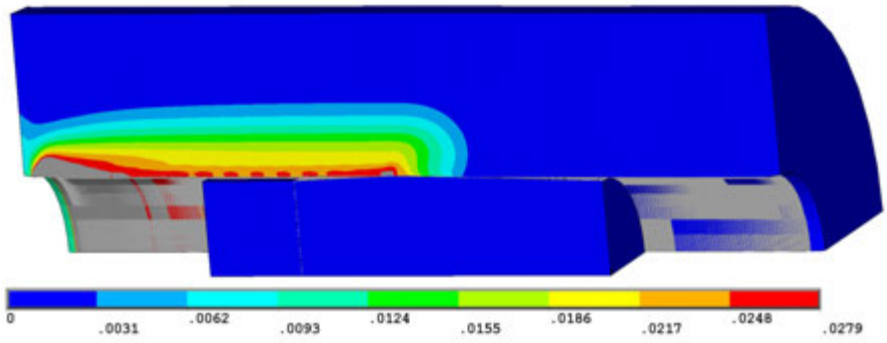

Figure 6: von Mises plastic strain distribution at the mid way of the swage autofrettage (2.5% interference with BE & friction).

process considering BE and friction for the case of 2.5% radial interference. By careful comparison, it can be found that an extremely high compressive radial stress field near the inner surface of the cylinder is initially being developed when the oversized mandrel is being pushed forward and making expansion in diameter of the cylinder in the contacting area, and then inducing a compressive residual radial stress on the inner surface and radial stress free on the outer surface of the cylinder after swage autofrettage (see Figure 5(a) and Figure 7(a)). Due to the compromise by the interaction in the contact area between the expansion driving force from the mandrel on inner surface and the expansion resistance from the outer layer, hoop stress is being developed in an opposite way throughout the wall-thickness, i.e., a very high compressive hoop stress near inner surface and a relative low tensile hoop stress towards outer surface, and finally resulting in a compressive residual hoop stress near inner layer, which is beneficial to cancelling the tensile hoop stress induced by working pressure (see Figure 4), and a tensile residual hoop stress near outer layer of the cylinder (see Figure 5(b) and Figure 7(b). Since swage autofrettage process is an axi-symmetric and dynamic stress-state deformation process in nature, the axial stress analysis is very important. As for most analytical solutions, plane stress assumption was adopted which resulted in a noticeable error. Moreover, as for experiments, real-time measurements could only be done on surface which made the measurements inadequate, and 3-D measurements, due to the sample preparation as aforementioned, were not reliable. From the modeling results, it can be seen that when the oversized mandrel is moving forward inside the cylinder and squeezing the inner surface material, combining the action from the friction, a high compressive axial stress near the inner surface and a tensile axial stress near the outer surface in the contacting area is being formed. Finally, a high compressive residual axial stress field near inner surface and a tensive residual axial stress field near outer surface of the cylinder is formed (see Figure5(c) and Figure7(c)), having a maximum compressive residual axial stress of about 57% value of the maximum compressive

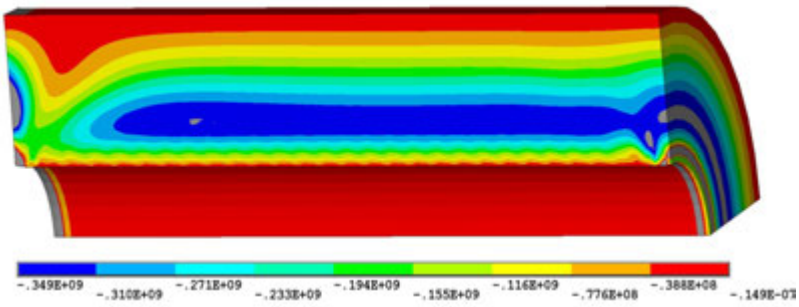

(a) Residual radial stress

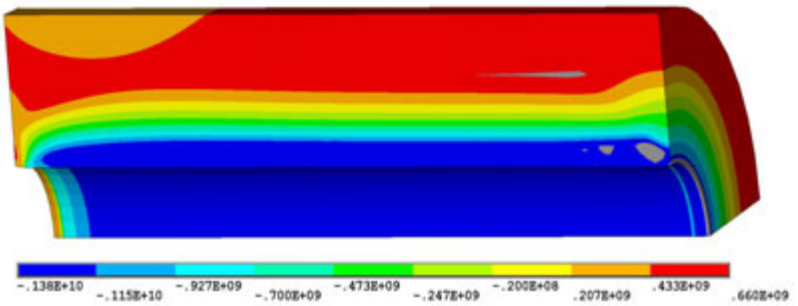

(b) Residual hoop stress

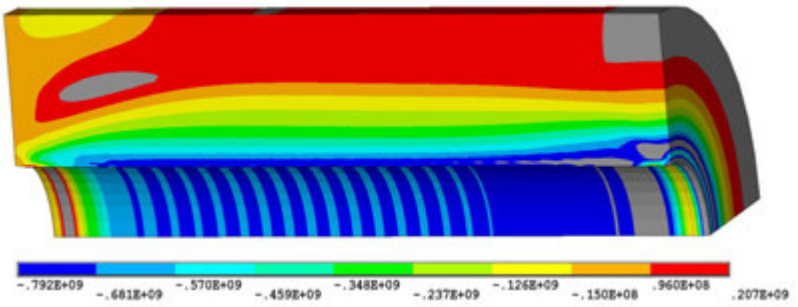

(c) Residual axial stress

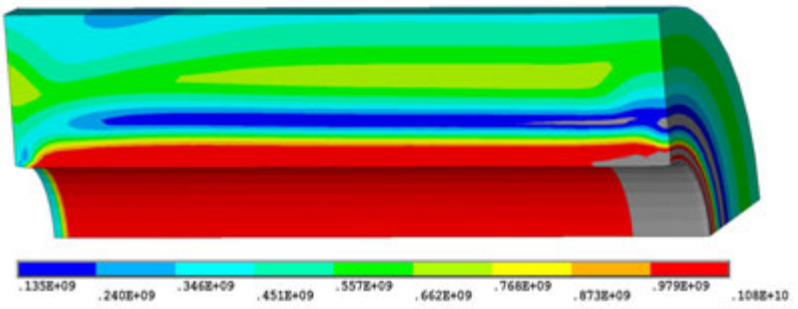

(d) Residual von Mises stress

(e)

Figure 7: Residual stress (Pa) distribution after swage autofrettage (2.5% interference with BE & friction).

*Corresponding author (**Z. Hu**). Tel/Fax: +1-605-688-4817/+1-605-688-5878. E-mail address: Zhong.Hu@sdstate.edu. Volume 3 No. 1 ISSN 2229-1652 eISSN 2229-1660 Online Available at http://TuEngr.com/ATEAS/V03/0031.pdf .

residual hoop stress and more than twice the maximum residual radial stress in the same area. von Mises stress is an equivalent stress indicator considering the contribution from each stress component. During the swage autofrettage process, von Mises stress in the contacting area on the inner surface is much higher than that on the outer surface, resulting in a higher residual von Mises stress field near inner surface and a lower one near outer surface of the cylinder. A very interesting phenomenon is that due to the transition of the compressive to tensive stress components from inner surface to outer surface, a minima of the residual von Mises is achieved inside the wall thickness of the cylinder (see Figure 5(d) and Figure 7(d)). Plastic deformation is firstly initiated from the inner surface in the contacting area and gradually expanded towards outer surface, so that the residual plastic strain field is the highest from inner surface to minima (zero) on outer surface with a maximum plastic strain of about 2.5% near inner surface (see Figures 6 and 8).

Overall, the residual stresses and strain in the central part of the length, i.e., about one wall-thickness length away from both ends, are well consistent and quite different from the end areas due to the minimal influence of the boundary conditions from both ends (see Figs. 7 and 8).

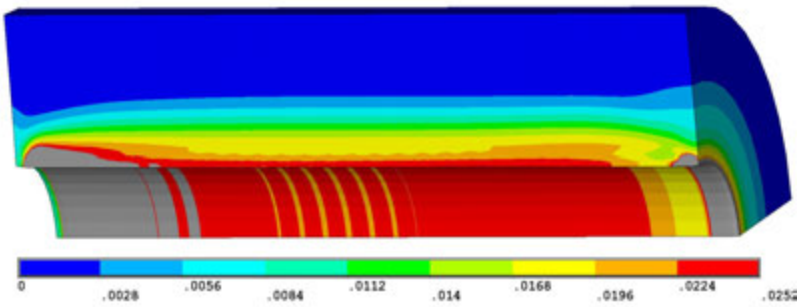

Figure 8: Residual von Mises plastic strain distribution after swage autofrettage (2.5% interference with BE & friction).

Figure 9 shows the modeling results of residual stress (radial, hoop, axial and von Mises) components at the mid-length of the cylinder changing throughout the wall-thickness after completing swage autofrettage process, considering BE and friction for different percent interference. It can be seen that residual radial stresses are free on both inner surface and outer surface of the cylinder, and compressive inside the wall-thickness. Higher interference induces higher compressive residual radial stress inside the wall (see Figure 9(a)). Residual hoop stresses are changing from compressive near the inner surface to tensile towards the outer surface of the

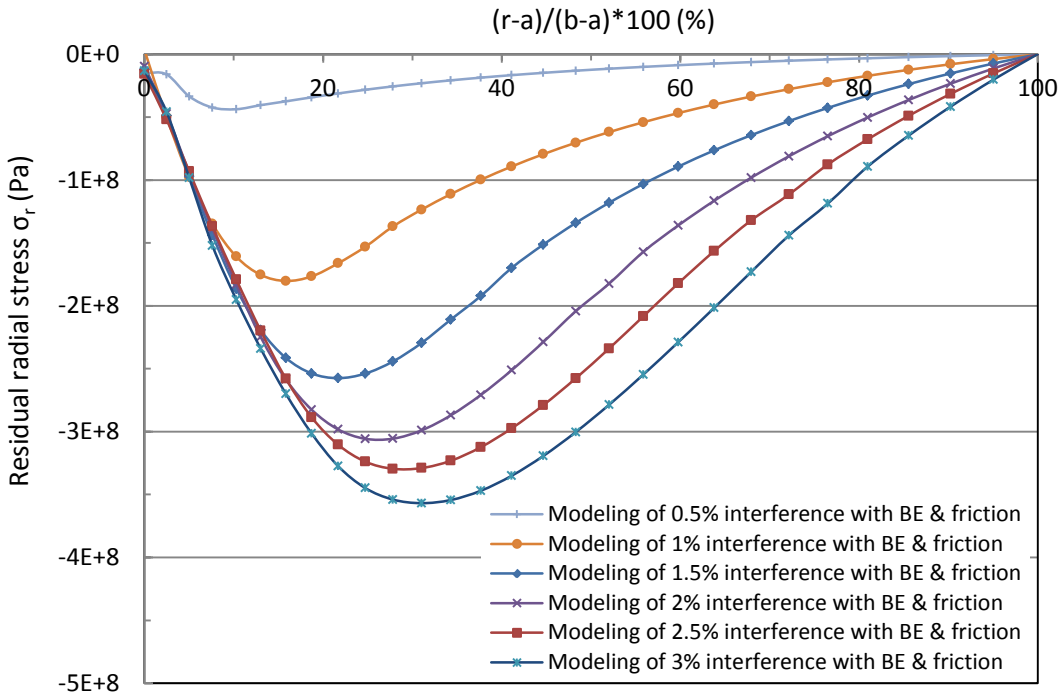

(a) Residual radial stress

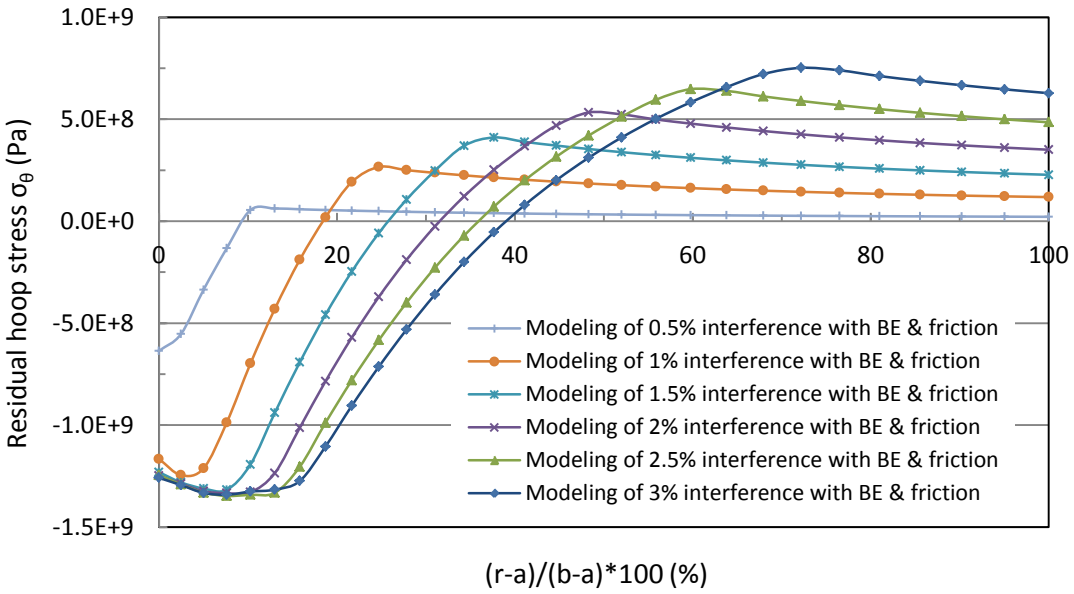

(b) Residual hoop stress

*Corresponding author (**Z. Hu**). Tel/Fax: +1-605-688-4817/+1-605-688-5878. E-mail address: Zhong.Hu@sdstate.edu. Volume 3 No. 1 ISSN 2229-1652 eISSN 2229-1660 Online Available at http://TuEngr.com/ATEAS/V03/0031.pdf .

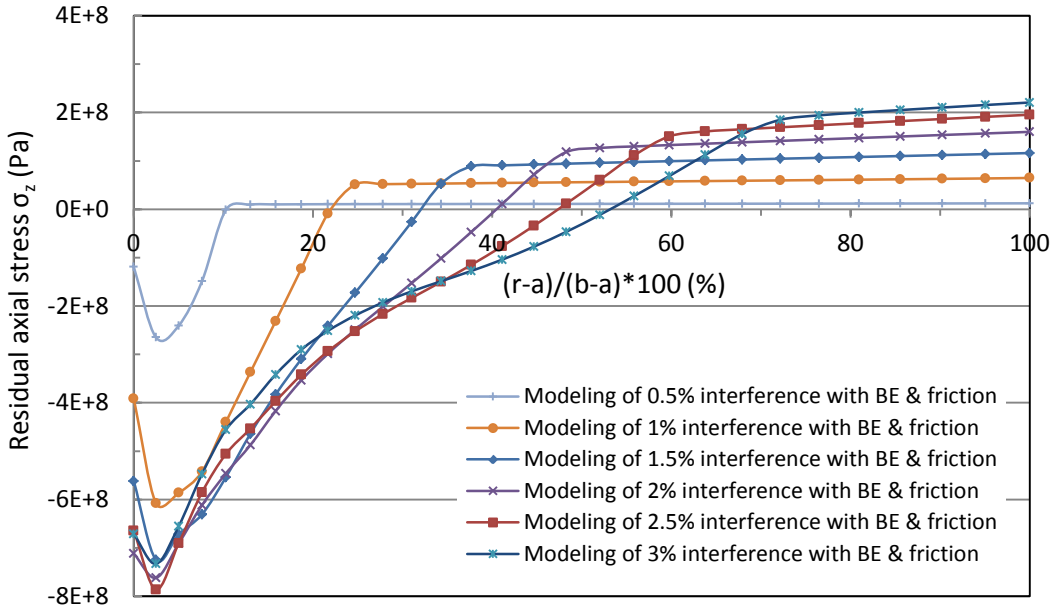

(c) Residual axial stress

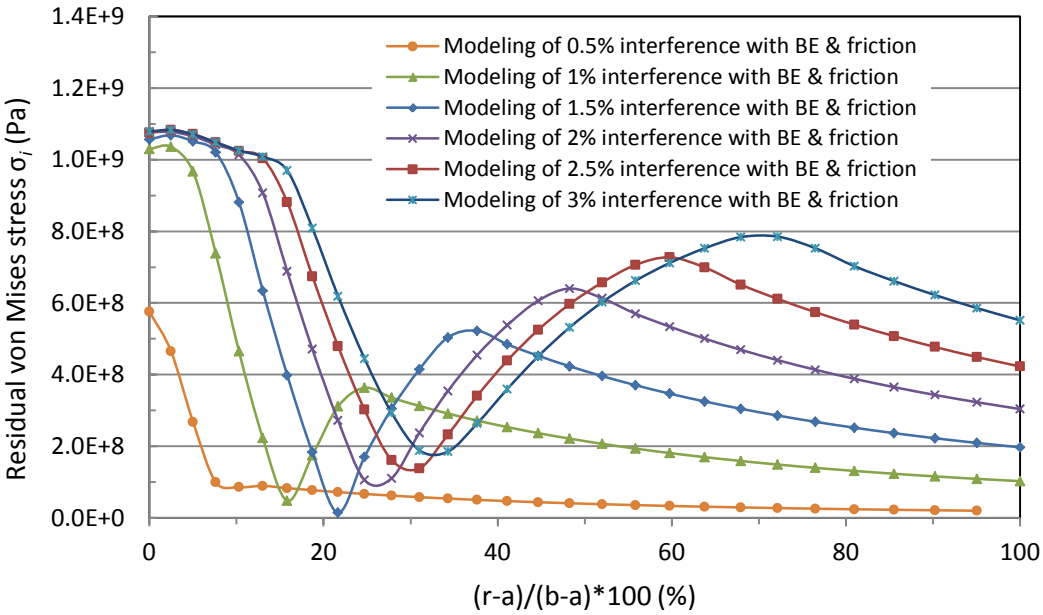

(d) Residual von Mises stress

Figure 9: Modeling residual stress distributions along wall-thickness at the mid-length of the cylinder after swage autofrettage under different interference percentage.

wall. Higher interference induces larger compressive area and higher tensile residual hoop stress. However, the maximum compressive residual hoop stress near the inner surface of the wall does not change significantly as interference increasing (see Figure 9(b)). Again, the compressive residual hoop stress will be beneficial to cancelling the tensile hoop stress induced by working

pressure. Similarly, residual axial stress are also changing from compressive near the inner surface to tensile near the outer surface of the wall, and higher interference induces larger compressive area and higher tensile residual axial stress, but maximum compressive residual axial stress is achieved at about 2.5% interference (see Figure 9(c)). For residual von Mises stress, near both inner surface and outer surface the stresses are much higher than inside the wall, and the minima is achieved inside the wall, due to the transition of the stresses from compressive to tensile (see Figure 9(d)).

Figure 10 shows the comparison of modeling results of residual stress (radial, hoop, axial and von Mises) components with experimental data [11] changing throughout the wall-thickness after completing swage autofrettage process, considering different modeling conditions (with or without BE or friction) for 2.5% interference and at the mid-length or near the mandrel inlet-end of the cylinder. As for residual radial stress, see Figure 10(a), considering BE or friction does not change significantly the stress value in the mid-length of the cylinder by modeling. As aforementioned, since the 3D measurements were not taken by real-time, cutting slices from the cylinder and machining and polishing slices into measurable samples made the residual stress change significantly (release or reorganize). It shows from modeling that the residual axial stress induced by swage autofrettage is at the same level as the residual hoop stress, and completely releasing axial stress on the sample surface will cause significant changes in other stresses. Therefore, the experimental data is not reliable for validation purpose. However, the stress distribution in the mid-length by modeling is quite different from near the mandrel inlet-end part where the stress distribution is closer to the experimental data, except near the outer surface where the residual radial stress was supposed to be vanished towards the outer surface. At this point, the experimental data of residual radial stress near the outer surface had noticeable error. As for residual hoop stress, see Figure 10(b), modeling results considering friction changes very little in the mid-length. However, considering BE reduces the compressive stress near the inner surface of the cylinder due to larger prior plastic strain. The stresses in the mid-length are quite different from the stress near the mandrel inlet-end. The trends of the modeling results are similar to the experimental data, except smaller by experiments. As for residual axial stress, see Figure 10(c), there is no axial stress in the case of experiments due to the free surface. Friction only influences the stress on the inner surface, and a compressive stress near the inner surface and a tensile stress towards the outer

*Corresponding author (**Z. Hu**). Tel/Fax: +1-605-688-4817/+1-605-688-5878. E-mail address: Zhong.Hu@sdstate.edu. Volume 3 No. 1 ISSN 2229-1652 eISSN 2229-1660 Online Available at http://TuEngr.com/ATEAS/V03/0031.pdf .

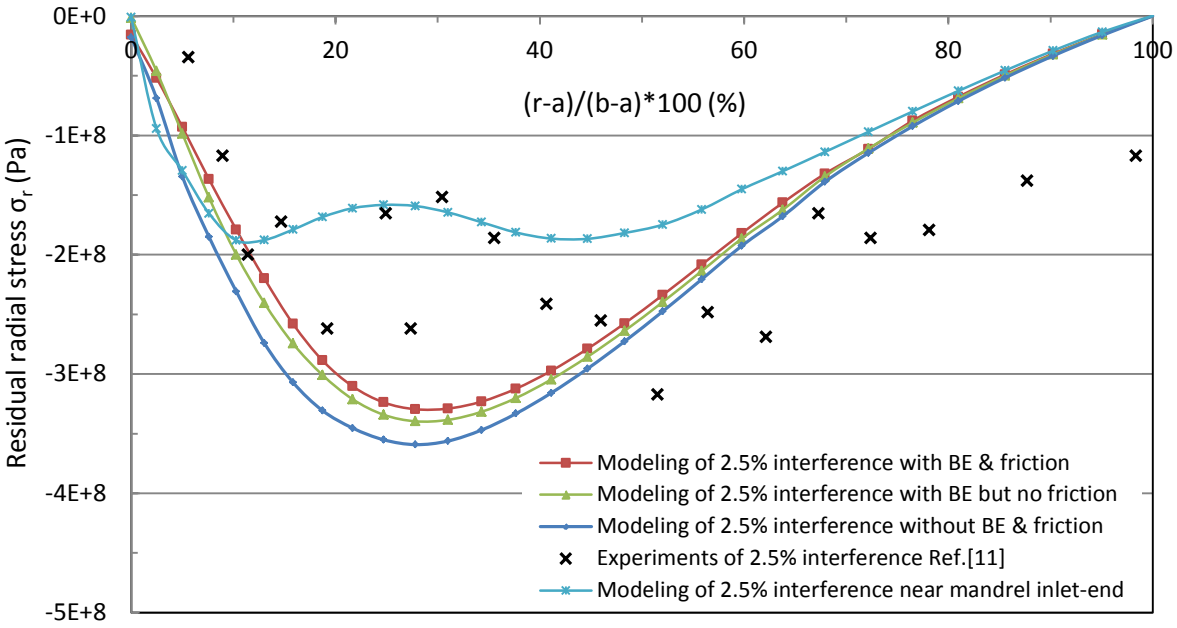

(a) Residual radial stress

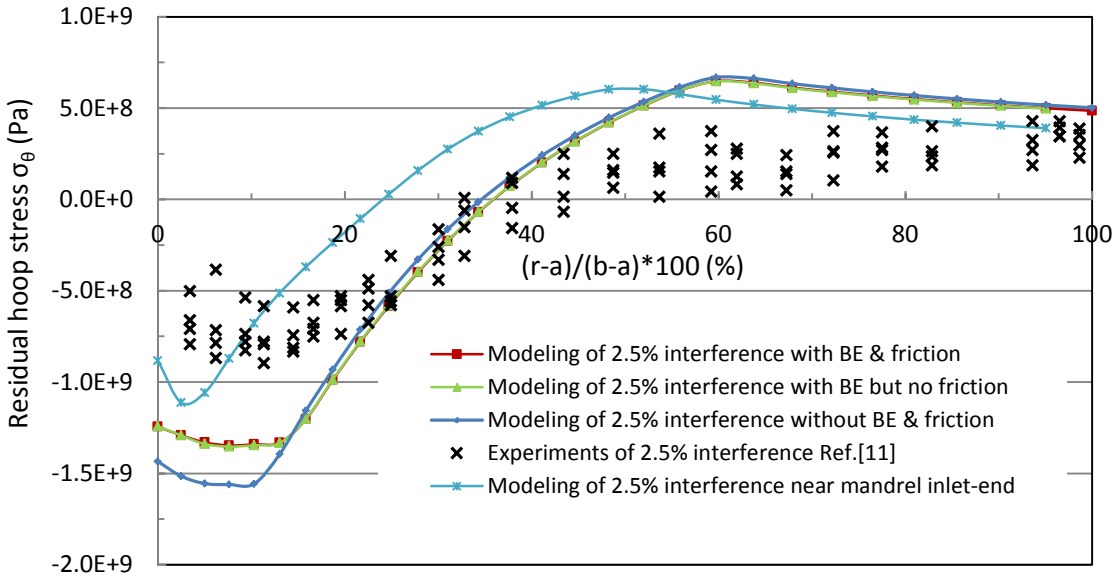

(b) Residual hoop stress

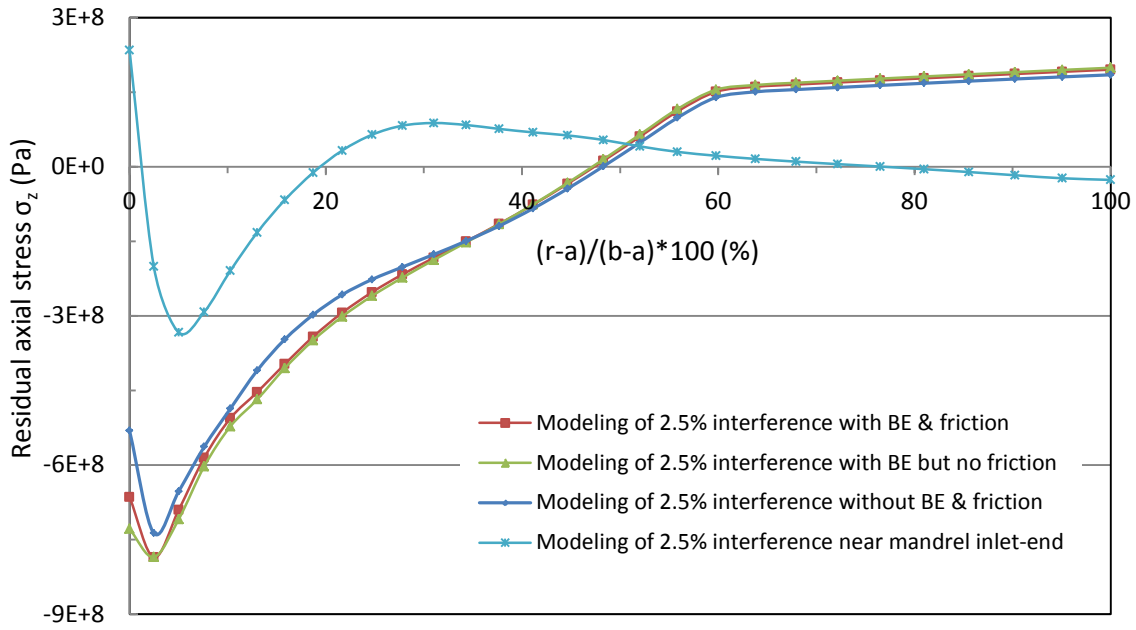

(c) Residual axial stress

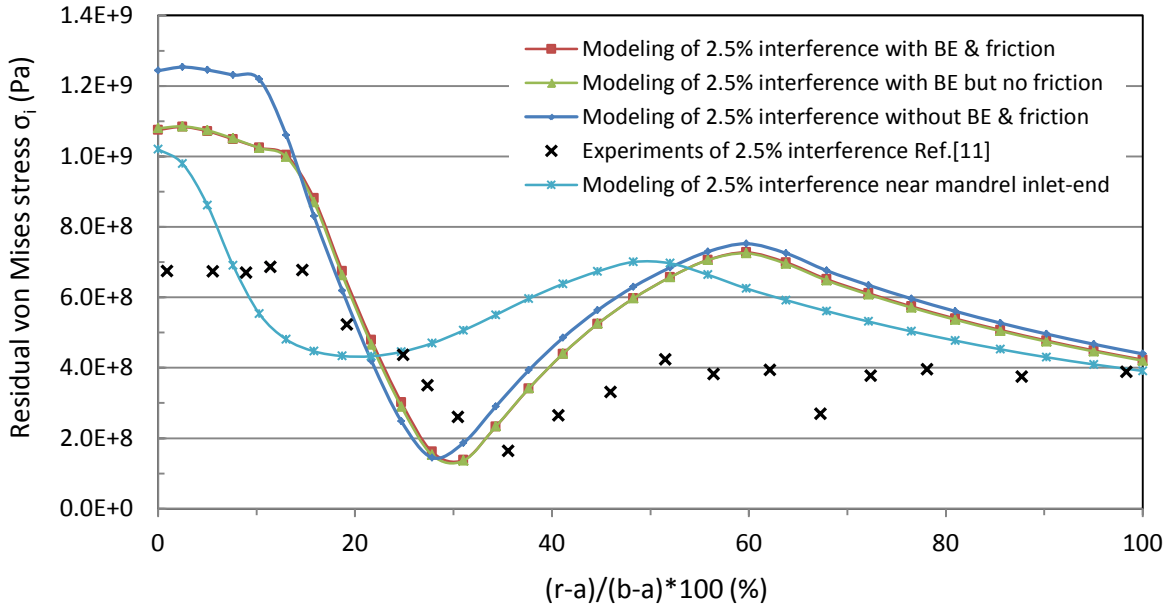

(d) Residual von Mises stress

Figure 10: Comparison of residual stresses by modeling with experiments for 2.5% interference swage autofrettage (modeling results other than indicated are taken from the mid-length of the cylinder).

*Corresponding author (**Z. Hu**). Tel/Fax: +1-605-688-4817/+1-605-688-5878. E-mail address: Zhong.Hu@sdstate.edu. Volume 3 No. 1 ISSN 2229-1652 eISSN 2229-1660 Online Available at http://TuEngr.com/ATEAS/V03/0031.pdf .

surface are presented by modeling. Again, the stress value in the mid-length is much higher than that near the mandrel inlet-end. For residual von Mises stress, see Figure 10(d), the experimental data were calculated from the stress components based on the plane stress condition. Generally speaking, friction does not significantly change the stress distribution. However, considering BE significantly lowers the stress value near the inner surface. The Stresses near the mandrel inlet-end are quite different from the stresses in the mid-length of the cylinder. Overall, the modeling results by considering BE and friction from this work are very close to the modeling results from [17].

Figure 11 shows the radial expansion of inner surface ($r=a$) and outer surface ($r=b$) of the cylinder vs. percent interference after swage autofrettage, considering BE and friction. It can be seen that the expansion on inner surface are over two and a half to three times the expansion on outer surface and the difference are getting less as percent interference increasing.

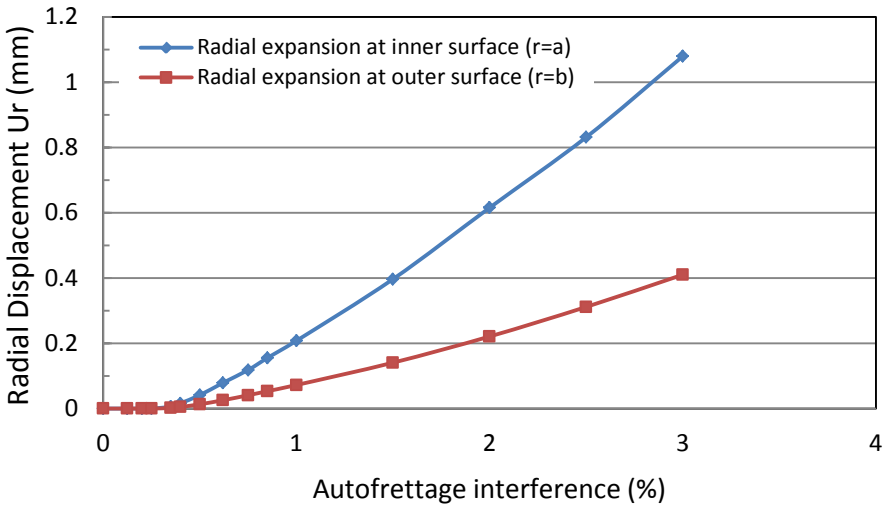

Figure 11: Radial expansion of the cylinder vs. percent interference (considering BE and friction).

4.3 Mandrel pushing forces during swage autofrettage

Mandrel pushing force is one of the very important parameters regarding swage autofrettage process design, and it can be used to select the load capability of the hydraulic system. Reducing pushing force can save energy and process/equipment cost, and prolong the mandrel life. Figure 12 shows the modeling pushing forces on mandrel by hydraulic ram when pushing oversized mandrel moving forward inside the cylinder during swage autofrettage process for different percent

interference, considering BE and friction. It is easy to understand that higher percent interference causes larger deformation and needs higher pushing force.

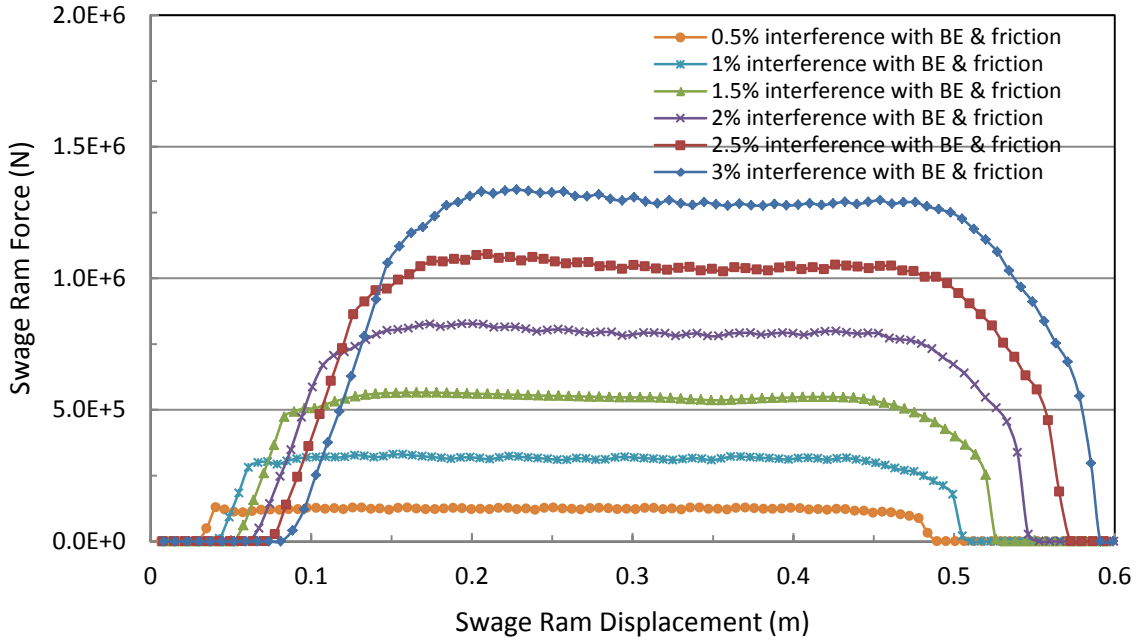

Figure 12: Pushing forces during swage autofrettage under different percent interference.

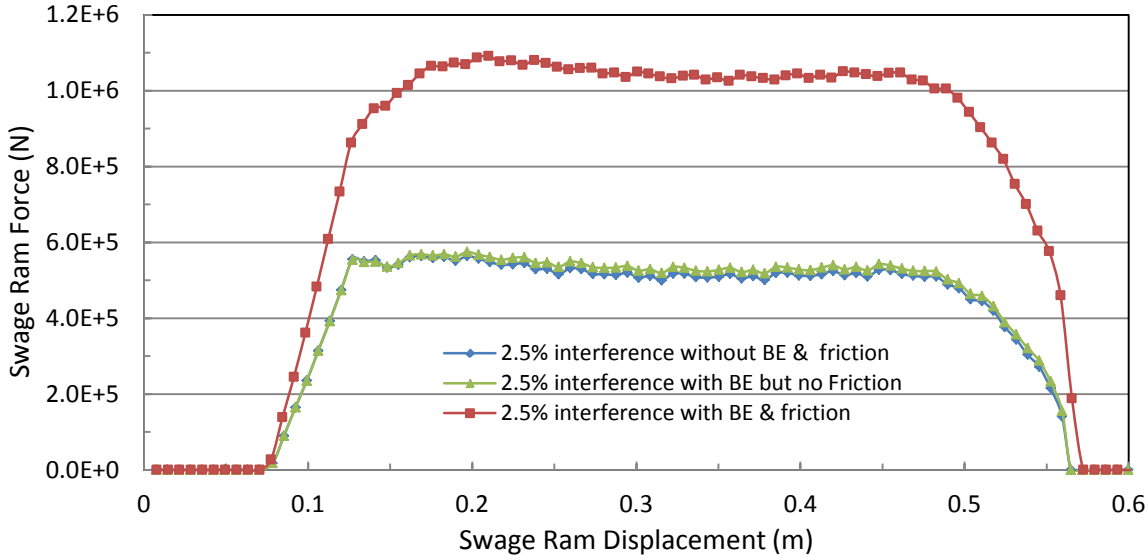

Figure 13: Pushing force comparison for 2.5% interference under different modeling conditions.

Figure 13 shows the pushing force comparison for 2.5% interference under different modeling conditions, i.e., with or without BE and friction. It can be seen that BE has little influence

*Corresponding author (Z. Hu). Tel/Fax: +1-605-688-4817/+1-605-688-5878. E-mail address: Zhong.Hu@sdstate.edu. Volume 3 No. 1 ISSN 2229-1652 eISSN 2229-1660 Online Available at http://TuEngr.com/ATEAS/V03/0031.pdf .

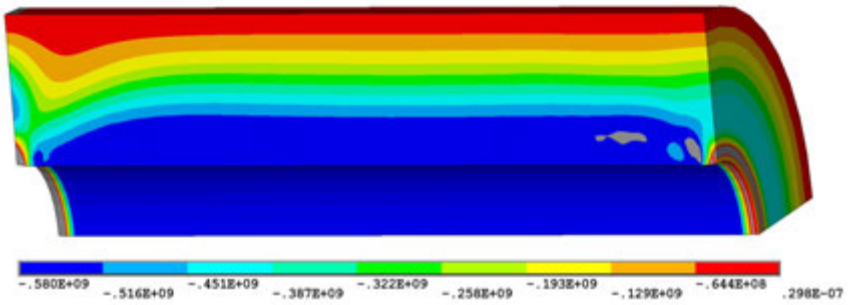

(a) Final radial stress

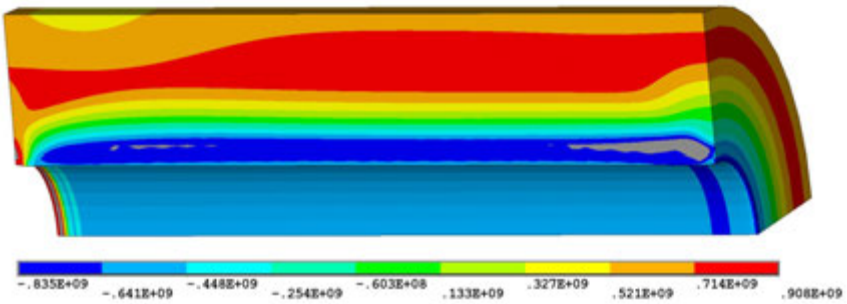

(b) Final hoop stress

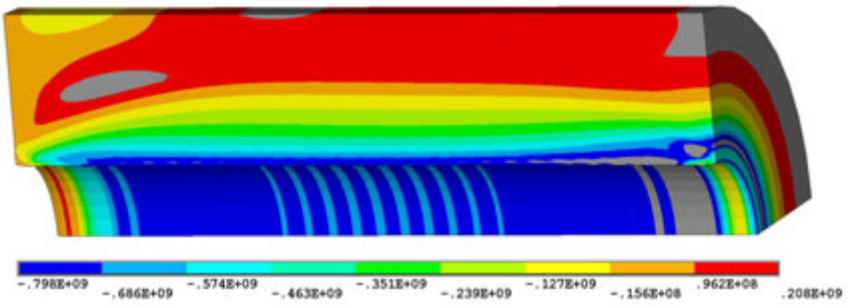

(c) Final axial stress

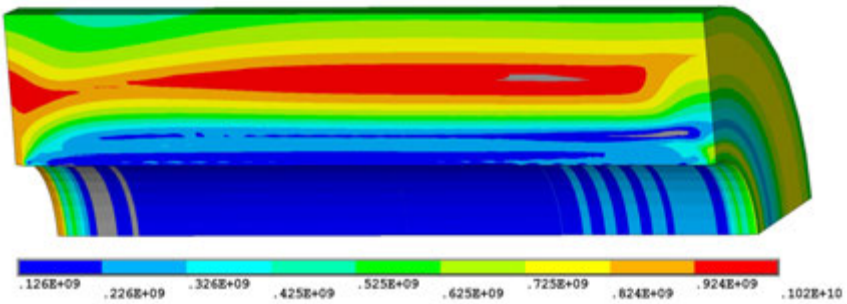

(d) Final von Mises stress

Figure 14: Final stress distribution under maximum working pressure (529.0 MPa and 2.5% interference with BE & friction).

on the pushing force. However, friction dramatically increases the pushing force which reminds the

designers and operators the importance of reducing friction from the surface preparation of the cylinder and the mandrel tools. The pushing force value with friction of about 1050kN, doubling the force without friction, is comparable with the experimental data from [13].

4.4 Final stresses under maximum internal working pressure

When a swage autofrettaged thick-walled cylinder is applied to an internal working pressure, this reloading pressurized process is basically treated as an elastic loading process, even though there is stress superimposing and cancellation happened, since plastic deformation is not desired in the application of the cylinders based on the static yield design criterion. Figure 14 shows the contour plots of the final stress distributions of a swage autofrettaged thick-walled cylinder after pressurized by an elastic-limit working pressure, i.e., the maximum working pressure of 529.0 MPa. It can be seen that final radial stress is of maximum compressive on the inner surface and gradually reduced throughout the wall-thickness to zero on the outer surface, see Figure 14(a). The final hoop stress is of maximum compressive near the inner surface which is beneficial to resisting failure and crack propagation initiated easily from inner surface. The final hoop stress changes from compressive on the inner surface to tensile on the outer surface throughout the wall-thickness, and the maximum tensile hoop stress is inside the wall in the center area, see Figure 14(b). The final axial stress changes from maximum compressive on the inner surface to maximum tensile on the outer surface throughout the wall-thickness (see Figure 14(c)). The combination of the stress components results in a minimal von Mises stress on the inner surface which is in favor of prolonging cylinder life, and a relative smaller value on outer surface, see Figure 14(d).

Again, the final stresses in the central part of the length are well consistent and quite different from both end areas, see Figure 14.

Figure 15 shows the modeling results of final stress (radial, hoop, axial and von Mises) components of a swage autofrettaged cylinder under a maximum working pressure at the mid-length changing throughout the wall-thickness, considering BE and friction for different percent interference. As for the final radial stress, by superimposing the residual stress, the compressive stress throughout the wall-thickness is increasing as percent interference increasing,

*Corresponding author (Z. Hu). Tel/Fax: +1-605-688-4817/+1-605-688-5878. E-mail address: Zhong.Hu@sdstate.edu. Volume 3 No. 1 ISSN 2229-1652 eISSN 2229-1660 Online Available at http://TuEngr.com/ATEAS/V03/0031.pdf .

see Figure 15(a). As for final hoop stress, the compressive stress near the inner layer as well as the tensile stress near the outer layer are increasing as the percent interference increasing, see Figure 15(b). As for the axial stress, the higher compressive stress is near the inner layer and the higher tensile stress is near the outer layer, see Figure 15(c). As for final von Mises stress, the maximum values where the yield failure initiates are presented from inner surface and moving towards outer surface as percent interference increasing, see Figure 15(d).

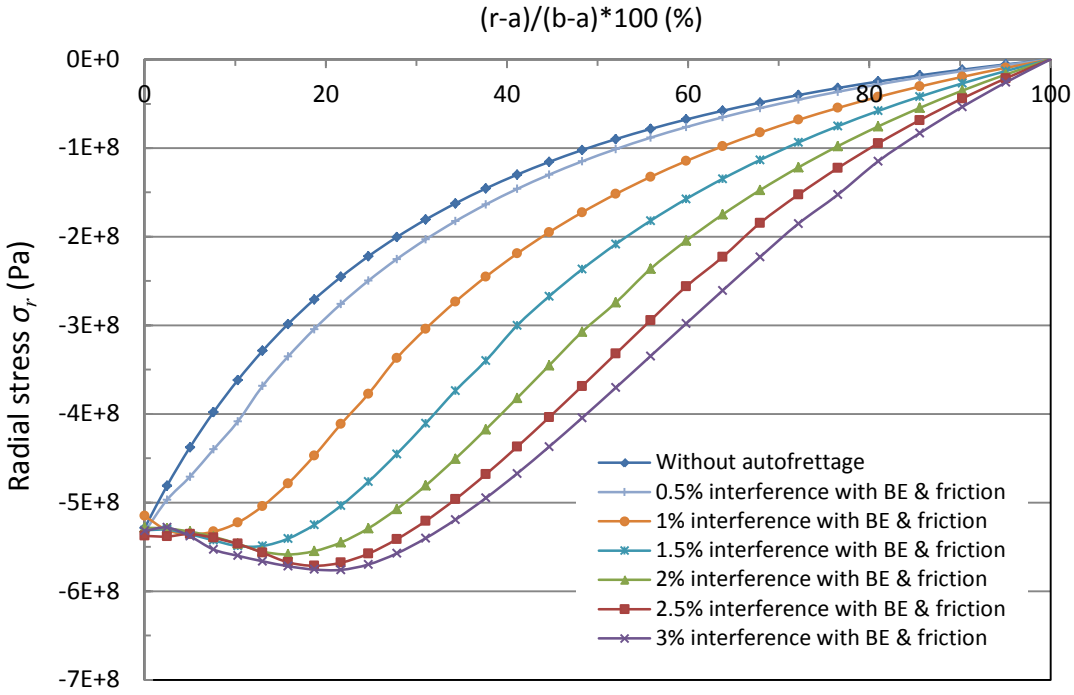

(a) Final radial stress

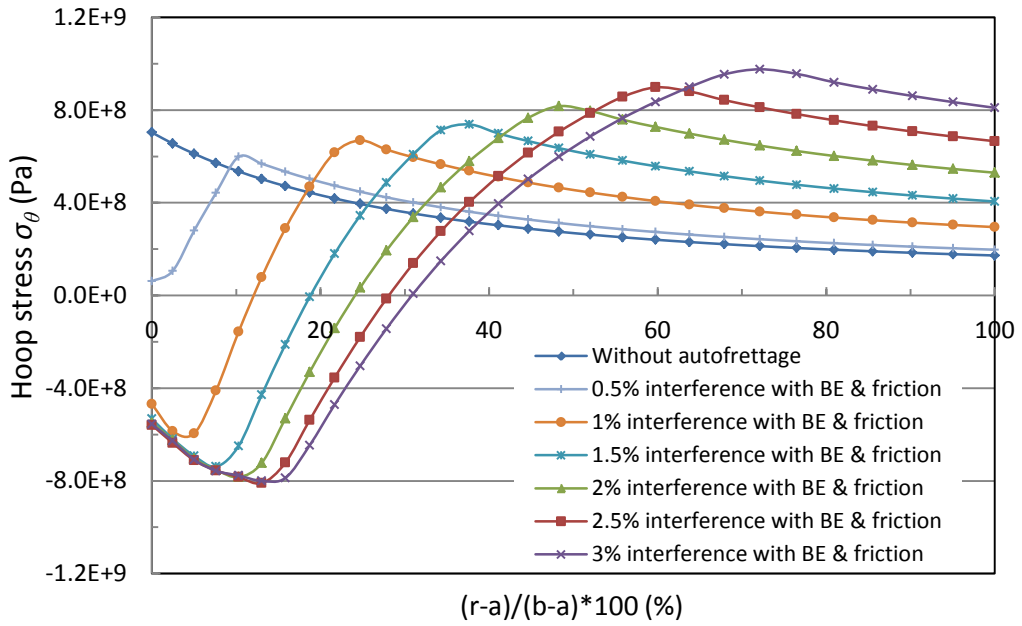

(b) Final hoop stress

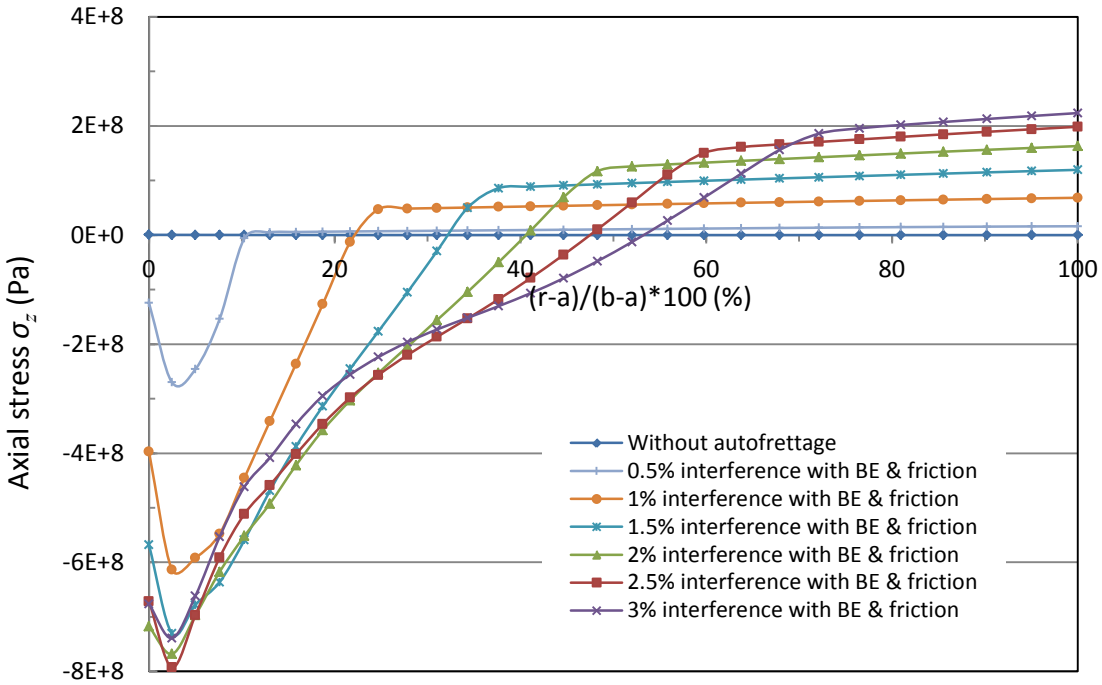

(c) Final axial stress

*Corresponding author (**Z. Hu**). Tel/Fax: +1-605-688-4817/+1-605-688-5878. E-mail address: Zhong.Hu@sdstate.edu. Volume 3 No. 1 ISSN 2229-1652 eISSN 2229-1660 Online Available at http://TuEngr.com/ATEAS/V03/0031.pdf .

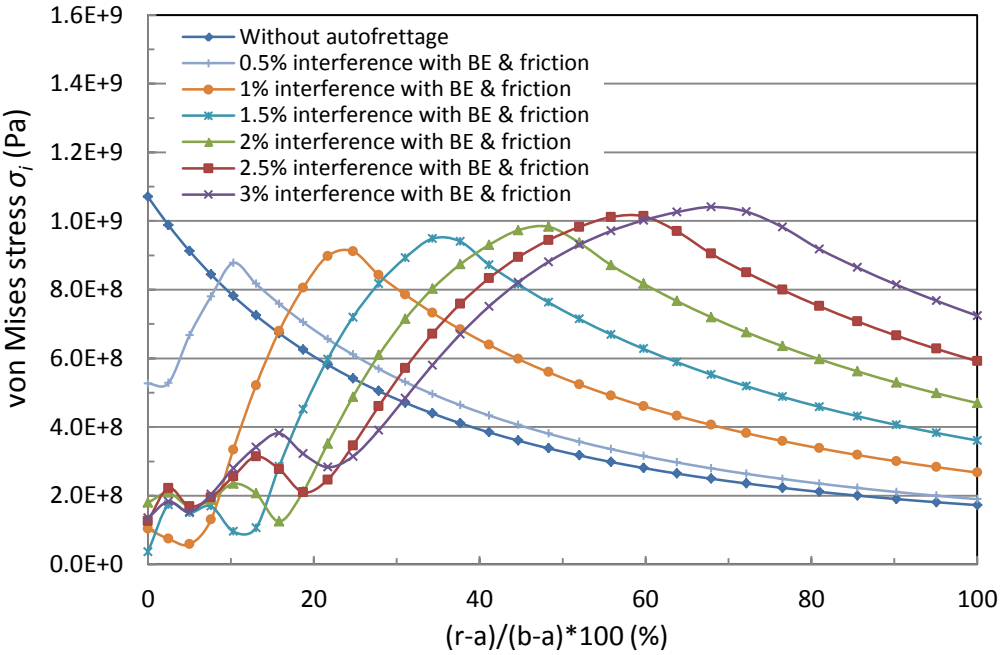

(d) Final von Mises stress

Figure 15: Modeling final stress distributions along wall-thickness at the mid-length of the cylinder under maximum working pressure for different percent interference.

Figure 16 shows the comparison of modeling results of final stress (radial, hoop, axial and von Mises) components at the mid-length changing throughout the wall-thickness under the maximum working pressure after 2.5% interference swage autofrettaged, considering different modeling conditions, i.e., with or without BE or friction. As for the final radial stress, BE and friction only slightly changes on the stress, see Figure 16(a). As for the final hoop stress, friction has little influence on the stress, but BE apparently changes the stress, see Figure16(b). As for the final axial stress, friction only changes the stress on the inner surface and BE significantly changes the stress, see Figure 16(c). As for the final von Mises stress, friction has little influence on the stress, but BE obviously changes the stress, see Figure 16(d).

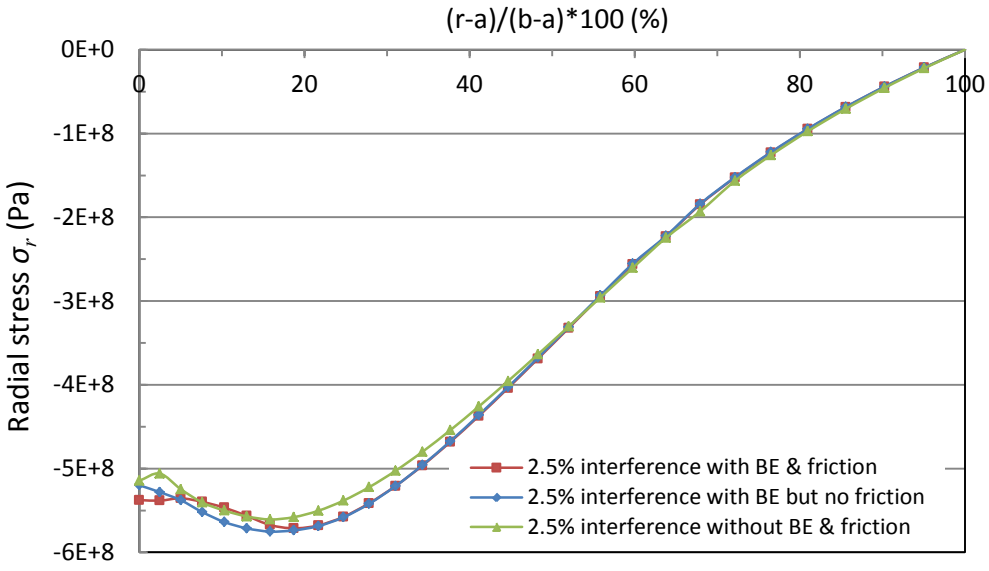

(a) Final radial stress

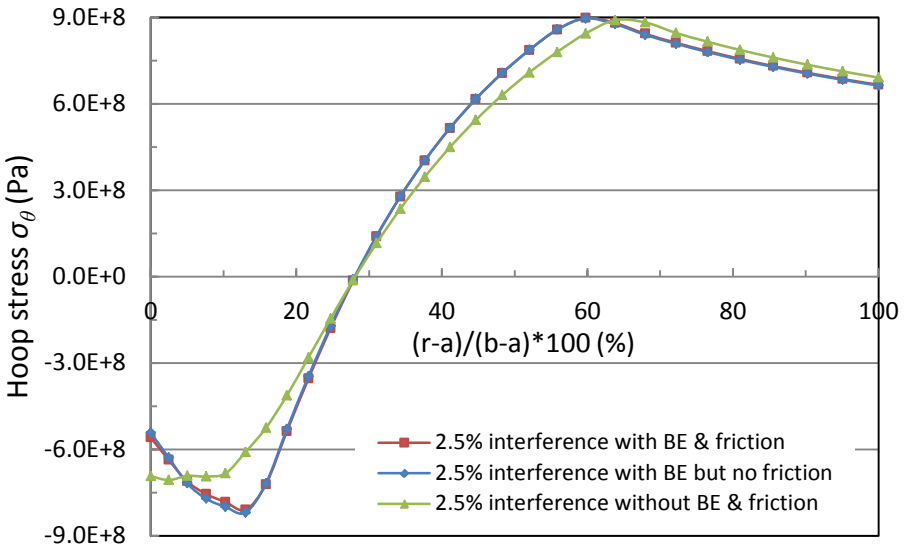

(b) Final hoop stress

*Corresponding author (**Z. Hu**). Tel/Fax: +1-605-688-4817/+1-605-688-5878. E-mail address: Zhong.Hu@sdstate.edu. Volume 3 No. 1 ISSN 2229-1652 eISSN 2229-1660 Online Available at http://TuEngr.com/ATEAS/V03/0031.pdf .

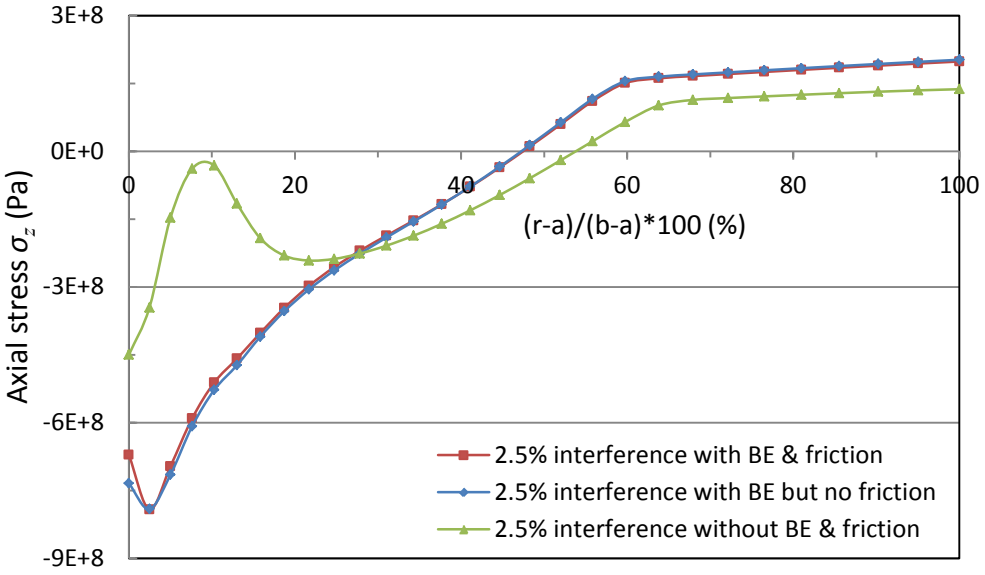

(c) Final axial stress

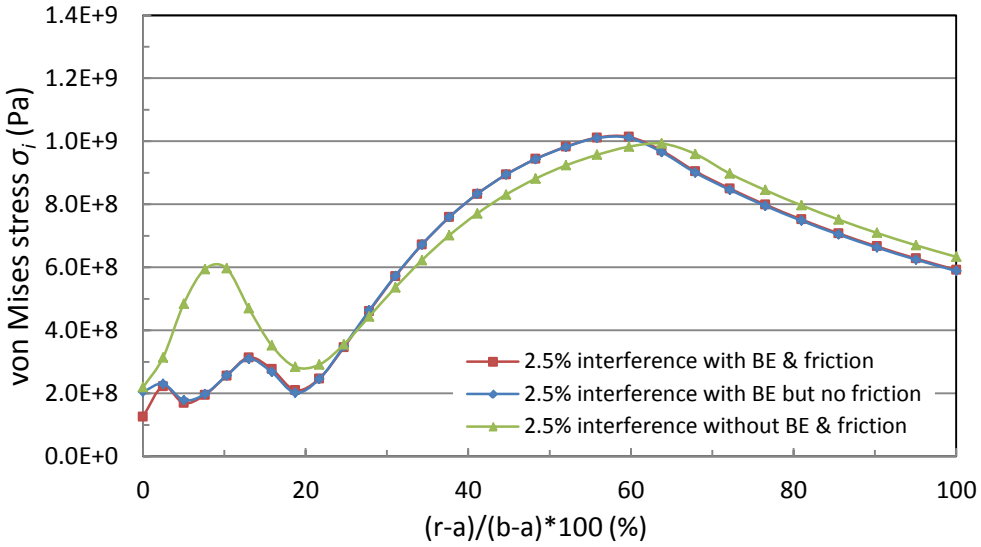

(d) Final von Mises stress

Figure 16: Comparison of final stress distribution along thickness under maximum working pressure by different modeling conditions after 2.5% interference swage autofrettaged (modeling results are taken from the mid-length of the cylinder).

Figure 17 shows the reduction of the final maximum von Mises stress by swage autofrettage under the maximum working pressure of 529.0 MPa. It clearly shows the optimal percent interference is about 0.62% for the given conditions, and the corresponding maximum von Mises stress reduction is about 18%.

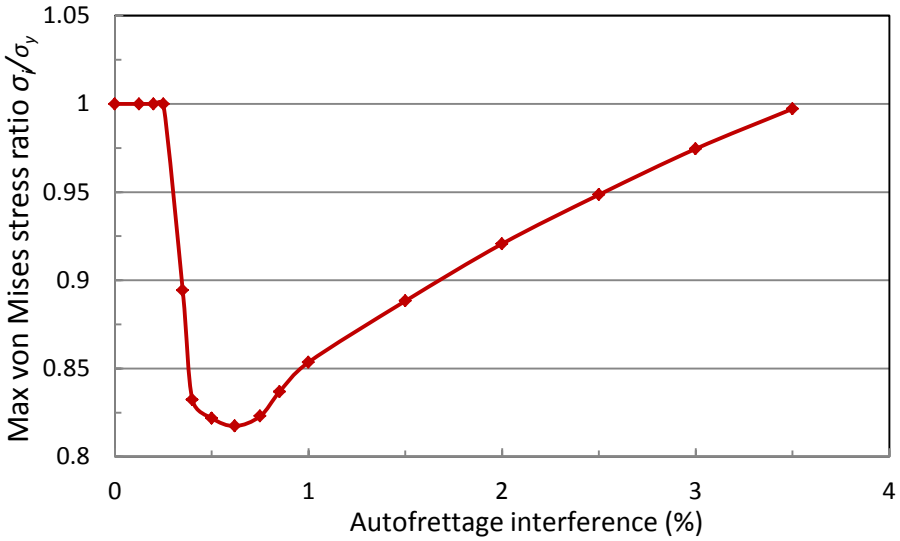

Figure 17: Reduction of final maximum von Mises stress under maximum working pressure for different percent interference (considering BE and friction).

5. Conclusion

The swage autofrettage processes of a thick-walled cylinder have been numerically investigated by finite element analysis, taking into account the elasto-plastic strain hardening material with kinematic hardening (the Bauschinger effect) and the von Mises yield criterion. The process optimization has been done by investigating the final stresses of the cylinder applying the maximum working pressure and changing the percent interference. The following conclusions have been reached:

It is necessary to consider the Bauschinger effect in the numerical modeling, since it has apparently influence on the stress state redistributions. The higher the percent interference, the larger the plastic strain induced and the greater the influence by Bauschinger effect is.

As for the stresses, friction on the contacting surface between the mandrel and the inner surface of the cylinder has little influence, except the axial stress on the inner surface of the cylinder. However, it has dramatically increased the swage ram pushing force.

For the given cylinder dimensions after swage autofrettage, there is optimized condition presented at about 0.62% radial interference, and the corresponding maximum von Mises stress reduction is about 18%.

*Corresponding author (**Z. Hu**). Tel/Fax: +1-605-688-4817/+1-605-688-5878. E-mail address: Zhong.Hu@sdstate.edu. Volume 3 No. 1 ISSN 2229-1652 eISSN 2229-1660 Online Available at http://TuEngr.com/ATEAS/V03/0031.pdf .

6. Acknowledgements

This work was supported by the State of South Dakota and Mechanical Engineering Department at South Dakota State University, and inspired by the Department of Defense project (Cooperative Agreement # W15QKN-09-2-0002) by METLAB at South Dakota State University. Computational facility technical support from Bryan Rieger at the University High Performance Computing, and the College of Engineering at South Dakota State University are gratefully acknowledged.

7. References

[1] Ford H, Watson E H, Crossland B. Thoughts on a code of practice for forged high pressure vessels of monobloc design. Journal of Pressure Vessel Technology, Transactions of ASME 1981; 103:2-8.

[2] Bundy M L, Conroy P J, Kennedy J L. Simulation & experimental in-wall temperature for 120 mm Ammunition. Defense Science Journal 1996;46 (4):223-232.

[3] Masu L M, and Craggs G. Fatigue strength of thick walled cylinders containing cross bores with blending features. Journal of Mech. Eng. Sci. 1992;206:299-309.

[4] Zapfec C A. Boiler embrittlement. Transactions of ASME (1942); 66(2): 81-126.

[5] Daniels F H. An interesting boiler explosion. Transactions of ASME 1942; 66(2): 81-126.

[6] Bush S H. Statistics of pressure vessels and piping failures. Journal of Pressure vessel Technology. 1988; 110: 225-233.

[7] Davidson T E, Barton C S, Reiner A N, Kendall D P. New approach to the autofrettage of high-strength cylinders, Experimental Mechanics 1962;2(2):33-40.

[8] Davidson T E, Kendall D P, Reiner A N. Residual stresses in thick-walled cylinders resulting from mechanically induced overstrain, Experimental Mechanics 1963;3(11):253-262.

[9] Davidson T E, Kendall D P. The design of pressure vessels for very high pressure operation, Mechanical Behavior of Materials Under Pressure, (Pugh H L P, Ed.) Elsevier Co. 1970.

[10] Malik M A, Khushnood S. A review of swage - autofrettage process. 11th International Conference on Nuclear Engineering. ICONE-11-36257 Tokyo, Japan, April 20-23, 2003:12pages.

[11] Lee S L. Residual stress analysis in swage autofrettaged thick-walled cylinders by position-sensitive x-ray diffraction techniques. US Army ARDEC Technical Report No. ARCCB-TR-94031. 1994.

[12] Lee S L, O'Hara G P, Olmstead V, Capsimalis G Characterization of residual stresses in an

eccentric swage autofrettaged thick-walled steel cylinder. US Army ARDEC Technical Report No. ARCCB-TR-92017. 1992.

[13] Perl M, Perry J. An experimental-numerical determination of the three-dimensional autofrettage residual stress field incorporating Bauschinger effects. Journal of Pressure Vessel Technology 2006;128:173-178.

[14] Perry J, Perl M. A 3-D model for evaluating the residual stress field due to swage autofrettage. Journal of Pressure Vessel Technology, Transactions of the ASME 2008;130:041211-1-6.

[15] Parker A P, O'Hara G P, Underwood J H. Hydraulic versus swage autofrettage and implications of the Bauschinger effect. Journal of Pressure Vessel Technology 2003;125:309-314.

[16] Alinezhad P. and Bihamta R. A study on the tool geometry effects in the swage autofrettage process. Advanced Materials Research. 2012;433-440:2206-2211.

[17] Gibson M C. Determination of residual stress distributions in autofrettaged thick-walled cylinders. Ph.D. Thesis. Granfield University April 2008.

[18] Venter A M, de Swardt R R, Kyriacon S. Comparative measurements on autofrettaged cylinders with large Bauschinger reverse yield zones. Journal of Strain Analysis 2000;35(6):459-469.

[19] Chaaban A. Static and fatigue design of high pressure vessels with blind-end and cross-bores, Ph.D. thesis, 1985, University of Waterloo, Waterloo, Ontario, Canada.

[20] Chaaban A, Leung K, Burns D J. Residual stress in autofrettaged thick-walled high pressure vessels. ASME PVP 1986;110:55-60.

[21] Kihiu J M, Mutuli S M, Rading G O. Stress characterization of autofrettaged thick-walled cylinders. International Journal of Mechanical Engineering Education 2003;31(4):370-389.

[22] Korsunsky A M. Residual elastic strains in autofrettaged tubes: elastic-ideally plastic model analysis. Journal of Engineering Materials and Technology 2007;129:77-81.

[23] Perry J, Aboudi J. Elasto-plastic stresses in thick walled cylinders. Transactions of the ASME 2003;125:248-252.

[24] Lazzarin P, Livieri P. Different solutions for stress and stress fields in autofrettaged thick-walled cylinders. Int. J. Pres. Ves. & Piping 1997;71:231-238.

[25] Huang X P. A general autofrettage model of a thick-walled cylinder based on tensile-compressive stress-strain curve of a material. The Journal of Strain Analysis for Engineering Design 2005;40:599-607.

[26] Hu Z, Puttagunta S. Computer modeling of internal pressure autofrettage process of a thick-walled cylinder with Bauschinger effect. American Transactions on Engineering & Applied Sciences, 2012;1(2):143-161.

*Corresponding author (**Z. Hu**). Tel/Fax: +1-605-688-4817/+1-605-688-5878. E-mail address: Zhong.Hu@sdstate.edu. American Transactions on Engineering & Applied Sciences. Volume 3 No. 1 ISSN 2229-1652 eISSN 2229-1660 Online Available at http://TuEngr.com/ATEAS/V03/0031.pdf .

[27] Iremonger M J, Kalsi G S. A numerical study of swage autofrettage. J. Pressure Vessel Technol. 2003;125(3):347-351.

[28] Bihamta R, Movahhedy M R, Mashreghi A R. A numerical study of swage autofrettage of thick-walled tubes. Materials & Design 2007;28(3):804-815.

[29] Malik M A, Khan M, Rashid B, Khushnood S. Analysis of swage autofrettage in metal tube. 14th International Conference on Nuclear Engineering. ICONE-14-89469 Miami, Florida, USA, July 17-20, 2006: 191-202.

[30] Troiano E, Underwood J H, Parker A P. Finite element investigation of Bauschinger effect in high-strength A723 pressure vessel steel. Journal of Pressure Vessel Technology, Transactions of the ASME, 2006; 128: 185-189.

[31] Milligan R V, Koo W H, Davidson T E. The Bauschinger Effect in a High Strength Steel. ASME J. Basic Eng., 1966;88:480-488.

[32] O'Hara G P. Analysis of the swage autofrettage process. US Army ARDEC Technical Report No. ARCCB-TR-92016. 1992.

[33] Venter A M, de Swardt R R, Kyriacou S. Comparative measurements on autofrettaged cylinders with large Bauschinger reverse yielding zones. J. Strain Anal. Eng. Des., 2000;35: 459-469.

[34] George D, Smith D J. The application of the deep hole technique for measuring residual stresses in an autofrettaged tube. PVP, High Pressure Technology, 2000;406: 25-31.

[35] Jahed H, Ghanbari G. Actual unloading behavior and its significance on residual stress in machined autofrettaged tubes. Journal of Pressure Vessel Technology, 2003; 125: 321-325.

[36] Jahed H, Farshi B, Karimi M. Optimum autofrettage and shrink-fit combination in multi-layer cylinders. Journal of Pressure Vessel Technology, 2006; 128: 196-200.

[37] Troiano E, Parker A P, Underwood J, Mossey C. Experimental data, numerical fit and fatigue life calculations relating to the Bauschinger effect in high strength armament steels. Journal of Pressure Vessel Technology, Transactions of the ASME, 2003;125: 330- 334.

[38] Troiano E, Parker A P, Underwood J H. Mechanisms and modeling comparing HB7 and A723 high strength pressure vessel steels. Journal of Pressure Vessel Technology, 2004; 126: 473-477.

[39] Perry J, Perl M, Shneck R, Haroush S. The influence of the Bauschinger effect on the yield stress, Young's modulus, and Poisson's ratio of a gun barrel steel. Journal of Pressure Vessel Technology, Transactions of the ASME, 2006; 128: 179-184.

[40] Perl M, Levy C, Rallabhandy V. The influence of the Bauschinger effect on 3D stress intensity factors for internal radial cracks in a fully or partially autofrettaged gun barrel. Journal of Pressure Vessel Technology, Transactions of the ASME, 2006; 128: 233-239.

[41] Huang X P, Cui W C. Effect of Bauschinger effect and yield criterion on residual stress distribution of autofrettaged tube. Journal of Pressure Vessel Technology, Transactions of

the ASME, 2006; 128: 212-216.

[42] Huang X, Moan T. Residual stress in an autofrettaged tube taking Bauschinger effect as a function of the prior plastic strain. Journal of Pressure Vessel Technology, Transactions of the ASME, 2009; 131: 021207(7 pages).

[43] Parker A P, Troiano E, Underwood J H, Mossey C. Characterization of steels using revised kinematic hardening model incorporating Bauschinger effect. Journal of Pressure Vessel Technology, Transactions of the ASME, 2003; 125: 277-281.

[44] Parker A P. Autofrettage of open end tubes - pressures, stresses, strains and code comparisons, Journal of Pressure Vessel Technology, 2001; 123:271-281.

[45] Underwood J H, deSwardt R R, Venter A M. Troiano E, Hyland E J, Parker A P. Hill Stress calculations for autofrettaged tubes compared with neutron diffraction residual stresses and measured yield pressure and fatigue life. ASME 2007 Pressure Vessels and Piping Conference (PVP2007-26617), 2007:47-52.

[46] ANSYS 13.0 User's Manual, Houston, Swanson Analysis System Inc., 2011.

[47] Ugural A C. Mechanics of Materials, John Wiley & Sons. Inc, NJ, 2008.

Dr. Zhong Hu is an Associate Professor of Mechanical Engineering at South Dakota State University. He received his BS and Ph.D. in Mechanical Engineering from Tsinghua University. He has worked for railway manufacturing industry as a senior engineer, Tsinghua University as a professor, Japan National Laboratory as a fellow, Cornell University, Penn State University and Southern Methodist University as a research associate. He has authored over 90 peer-reviewed publications in the journals, proceedings and book chapters in the areas of nanotechnology and nanoscale modeling by quantum mechanical/molecular dynamics (QM/MD); development of renewable energy related materials; mechanical strength evaluation and failure prediction by finite element analysis (FEA) and nondestructive engineering (NDE); design and optimization of advanced materials (such as biomaterials, carbon nanotube, polymer and composites).

Chandra Penumarthy has received his Bachelor's degree in Mechanical Engineering from Jawaharlal Nehru Technological University in India (2003-2007), and Master's degree in Mechanical Engineering from South Dakota State University, Brookings, SD, USA (2008-2011). He is currently Product Engineer at Ford Motor Company, Dearborn, MI, USA (April 2012-present).

Peer Review: This article has been internationally peer-reviewed and accepted for publication according to the guidelines given at the journal's website.

*Corresponding author (**Z. Hu**). Tel/Fax: +1-605-688-4817/+1-605-688-5878. E-mail address: Zhong.Hu@sdstate.edu. American Transactions on Engineering & Applied Sciences. Volume 3 No. 1 ISSN 2229-1652 eISSN 2229-1660 Online Available at http://TuEngr.com/ATEAS/V03/0031.pdf .